An optimal-control-based framework for trajectory planning, threat assessment, and semi-autonomous control of passenger vehicles in hazard avoidance scenarios

Sterling J. Anderson and Steven C. Peters

Department of Mechanical Engineering,
Massachusetts Institute of Technology,
77 Massachusetts Ave.,
Cambridge, MA 02139, USA
E-mail: ster@mit.edu
E-mail: scpeters@mit.edu

Tom E. Pilutti

Ford Research Laboratories,
Dearborn, MI 48124, USA
E-mail: tpilutti@ford.com

Karl Iagnemma*

Department of Mechanical Engineering,
Massachusetts Institute of Technology,
77 Massachusetts Ave.,
Cambridge, MA 02139, USA
E-mail: kdi@mit.edu
*Corresponding author

Abstract: This paper formulates the vehicle navigation task as a constrained optimal control problem with constraints bounding a traversable region of the environment. A model predictive controller iteratively plans an optimal vehicle trajectory through the constrained corridor and uses this trajectory to establish the minimum threat posed to the vehicle given its current state and driver inputs. Based on this threat assessment, the level of controller intervention required to prevent departure from the traversable corridor is calculated and driver/controller inputs are scaled accordingly. Simulated and experimental results are presented to demonstrate multiple threat metrics and configurable intervention laws.

Keywords: semi-autonomous control; shared-adaptive control; threat assessment; hazard avoidance; active safety; vehicle autonomy; model predictive control; MPC; model predictive control; lane keeping; human-in-the-loop; autonomous systems.

Reference to this paper should be made as follows: Anderson, S.J., Peters, S.C., Pilutti, T.E. and Iagnemma, K. (2010) 'An optimal-control-based framework for trajectory planning, threat assessment, and semi-autonomous control of passenger vehicles in hazard avoidance scenarios', *Int. J. Vehicle Autonomous Systems*, Vol. 8, Nos. 2/3/4, pp.190–216.

Biographical notes: Sterling J. Anderson is a Doctoral Candidate and National Defense Science and Engineering Graduate (NDSEG) Fellow at the Massachusetts Institute of Technology. Since joining the MIT Robotic Mobility Group in 2007, he has been developing new methods for trajectory planning, threat assessment, and semi-autonomous control of passenger vehicles. The framework presented in this paper is one outgrowth of this research. He received his BS from Brigham Young University in 2007 and his MS from MIT in 2009.

Steven C. Peters received his Bachelor's Degree in Mechanical Engineering from the University of California, Davis in 2004, and his MS from the MIT in 2006. He is currently a Research Assistant working towards his PhD at the MIT. His research interests include simulation and control of robotic vehicles, with a particular focus on rollover stability and hazard avoidance, and the development of efficient energy and transportation systems. He is a member of IEEE and SAE.

Tom E. Pilutti is a Technical Expert at Ford Motor Company specialising in active safety system design and development. He holds a BS from Purdue University and an MS and PhD from the University of Michigan.

Karl Iagnemma is a Principal Research Scientist in the Mechanical Engineering Department at the MIT. He holds a BS from the University of Michigan, and an MS and PhD from MIT, where he was a National Science Foundation Graduate Fellow. He has performed postdoctoral research at MIT, and has been a Visiting Researcher at the NASA Jet Propulsion Laboratory and the National Technical University of Athens (Greece). His primary research interests are in the areas of design, sensing, motion planning, and control of mobile robots in outdoor terrain, including modelling and analysis of robot-terrain interaction.

1 Introduction

Recent traffic safety reports from the National Highway Traffic and Safety Administration show that in 2007 alone, over 41,000 people were killed and another 2.5 million injured in motor vehicle accidents in the USA (National Highway Traffic Safety Administration (NHTSA), 2008). The longstanding presence of passive safety systems in motor vehicles, combined with the ever-increasing influence of active systems, has contributed to a decline in these numbers from previous years. Still, the need for improved collision avoidance technologies remains significant.

Passenger safety in human-controlled motor vehicles has historically focused on *passive safety* systems. Such systems, which include seat belts, air bags, and crumple zones, concentrate primarily on mitigating the effects of collisions on passengers. In recent years, the focus of motor vehicle safety has shifted from simply minimising the damage caused by collisions to avoiding accidents altogether. With the advent of anti-lock brakes, electronic stability control, and adaptive cruise control,

these *active safety* systems have begun to play a major role in collision mitigation (McBride et al., 2008).

Recent developments in onboard sensing and drive-by-wire capabilities have facilitated the development of active safety systems that share steering and/or braking control with the driver. These active safety systems operating with a "human in the loop" generally attempt to honour driver intentions, opposing them only when doing otherwise would lead to a collision or loss of control. Such modification of the driver's intended trajectory requires that these systems assess the threat posed to a vehicle in order determine when and how strongly to intervene. Such systems should honour safe driver inputs and manoeuvres while intervening when necessary to correct or override those deemed unsafe. This intervention should strike a necessary balance between the level and frequency of intervention: not altering the driver's steering and braking inputs 'too much', 'too soon', or 'too often' while still guaranteeing that the vehicle avoid hazards independent of that driver input.

1.1 Previous work

In recent years, extensive research has focused on intelligent vehicle navigation. Many warning, intervention (driver-assistance or semi-autonomous control), and autonomous control schemes have been developed to perform lateral and longitudinal vehicle guidance (McBride et al., 2008; Falcone et al., 2008a; Pohl et al., 2007; Weilkes et al., 2005). Supporting technologies such as onboard sensing, lane detection techniques, and obstacle recognition algorithms have also been proposed and implemented in test vehicles (Liu et al., 2007; Leonard et al., 2008; Guo et al., 2006; Fritsch et al., 2008).

As described in Calhoun and Queen (2002), Wei-Min and Bayard (1999), Cremean et al. (2006) and Smith et al. (2000), the autonomous vehicle guidance system may be broken down into three main tasks: trajectory generation, trajectory re-planning, and low-level control. The trajectory generation task pre-computes the vehicle trajectory. This may be performed online or offline. The low-level control system seeks to track the path generated by the trajectory re-planner using any of a multitude of vehicle actuation modes (front and rear steering, differential braking, active suspension, engine torque, etc.). While the low-level controller is not required to share the same vehicle or environmental model as the trajectory re-planner (Thrun et al., 2006), recent work in autonomous vehicle control using Model Predictive Control (MPC) has shown that using similar models for trajectory re-planning and low-level control can improve the guidance, navigation, and control system's path-tracking performance (Borrelli et al., 2005; Falcone et al., 2008b).

In Mobus and Zomotor (2005), a corridor – as opposed to a specific path – is preselected and a Finite Horizon Constrained Optimal Controller (FHCOC) is used perform both the re-planning and low-level control tasks required to keep the vehicle within the safe corridor while satisfying input constraints, safety constraints, and ride comfort preferences. This approach reduces the path planning task to the simpler task of corridor selection and merges the path re-planning and low level control tasks into the same control calculation. Furthermore, because the corridor selection in this approach does not plan a specific vehicle trajectory, the 're-planning' task performed online by the model predictive controller may be more clearly described as an online trajectory 'plan'.

Fully-autonomous vehicle navigation techniques have been developed to track pre-defined trajectories (Falcone et al., 2008a; Besselmann and Morari, 2008), travel

within lane markings (Liu et al., 2007; Mobus and Zomotor, 2005; Sattel and Brandt, 2008), or avoid obstacles (Jansson, 2005) via front wheel steering (Borrelli et al., 2005; Alleyne, 1997b), rear wheel steering (Falcone et al., 2007a; Ackermann, 1994), four-wheel-steering (Alleyne, 1997a), and differential brake steering (Falcone et al., 2008c; Pilutti et al., 1995). Control laws employed in these systems include PID schemes (Cremean et al., 2006), linear-quadratic regulators (Bemporad et al., 2002), and finite-horizon constrained optimal controllers (Mobus and Zomotor, 2005).

Among existing proposals for semi-autonomous vehicle navigation, lane-keeping systems using audible warnings (Jansson, 2005; Zheng et al., 2004), haptic alerts (Pohl et al., 2007; Brandt et al., 2007), steering torque overlays (Mobus and Zomotor, 2005; Pilutti and Ulsoy, 1999), and various combinations of these have been developed with mixed results (Pohl et al., 2007). In a recent subproject of the European PReVENT consortium, a lane-keeping system was designed to prevent lane departure by perceiving the environment, making heuristic-based trajectory planning decisions based on perceived threat, and implementing warning mechanisms or slight steering torque overlay when the vehicle drifts from the desired trajectory (Netto et al., 2006).

Many of the navigation systems developed in previous work address only one piece of the active safety problem. While some use rapidly-exploring random trees (Leonard et al., 2008; Tan et al., 2007), evolutionary programming (Vaidyanathan et al., 2001) or potential fields (Tsourveloudis et al., 2001; Rossetter and Christian Gardes, 2006) to plan a safe vehicle path, others simply begin with this path presumed (Alleyne, 1997a; Falcone et al., 2007b). The threat posed by a particular path is seldom assessed by the controller itself and is often only estimated by a simple threat metric such as lateral vehicle acceleration required to avoid a road hazard (Engelman et al., 2006). Finally, hazard avoidance is commonly performed using one or more actuation methods (steering, differential braking, etc.) without explicitly accounting for the effect of driver inputs on the vehicle trajectory (Netto et al., 2006). Such controllers selectively replace (rather than assist) the driver in performing the driving task.

Yu addressed this problem in mobility aids for the elderly by designing an adaptive shared controller which allocates control authority between the human user and a controller in proportion to the user's performance (Yu et al., 2003). These metrics and the associated intervention are designed to act on current and past user performance, however, and do not anticipate future deviations, tip over margins, or distances to obstacles. This reactive approach to semi-autonomy, while sufficient to control low speed mobility aids, is not well suited for higher speed applications with significant inertia effects and no pre-planned trajectory.

1.2 Current work

This paper describes the design of a passenger vehicle active safety framework that performs trajectory planning, threat assessment, and hazard avoidance in a unified manner. This framework leverages the predictive- and constraint-handling capabilities of MPC to plan trajectories through a pre-selected corridor, assess the threat this path poses to the vehicle, and regulate driver and controller inputs to maintain the threat below a given threshold.

Section 2 describes the semi-autonomous control framework and its associated trajectory prediction, control law, threat assessment, and intervention law. Section 3

discusses simulation setup and results, followed by experimental setup and results in Section 4. Finally, the paper concludes with general conclusions in Section 5.

2 Framework description

The framework described below leverages the predictive- and constraint-handling capabilities of MPC to perform trajectory planning, threat assessment, and hazard avoidance. First, an objective function is established to capture desirable performance characteristics of a safe or 'optimal' vehicle path. Boundaries tracing the edges of the drivable road surface are assumed to have been derived from forward-looking sensor data and a higher-level corridor planner. These boundaries establish constraints on the vehicle's projected position. This constraint data, together with a model of the vehicle dynamics is then used to calculate an optimal sequence of inputs and the associated vehicle trajectory. The predicted trajectory is assumed to be a 'best-case' scenario and used to establish the minimum threat posed to the vehicle given its current state and a series of best-case inputs. This threat is then used to calculate the necessary intervention required to prevent departure from the traversable region of travel and driver/controller inputs are scaled accordingly. Figure 1 shows a block diagram of this system.

Figure 1 Diagram of the active safety system (see online version for colours)

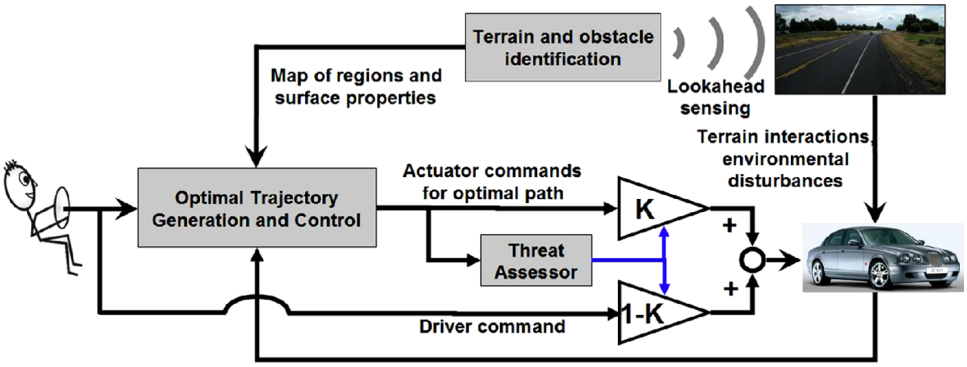

2.1 Assumptions

In this paper it is assumed that road lane data is available and that road hazards have been detected, located, and mapped into a 2-dimensional corridor of travel. Existing systems and previous work in onboard sensing and sensor fusion justify this as a reasonable assumption (Guo et al., 2006; Lemelson and Pedersen, 1999). Radar, LIDAR, and vision-based lane-recognition systems (McBride et al., 2008; Leonard et al., 2008; Fritsch et al., 2008), along with various sensor fusion approaches (Zomotor and Franke, 1997; Fritz et al., 2004) have been proposed to provide the lane, position, and environmental information needed by this framework.

Additionally, where multiple corridor options exist (such as cases where the roadway branches or the vehicle must circumnavigate an obstacle in the centre of the lane), it is assumed that a high-level path planner has selected a single corridor through which the vehicle should travel.

2.2 Path planning

The best-case (or baseline) path through a given region of the state space is established by a model predictive controller. Model predictive control is a finite-horizon optimal control scheme that iteratively minimises a performance objective defined for a forward-simulated plant model subject to performance and input constraints (Bemporad et al., 2002; Garcia et al., 1989; Camacho and Bordons, 2004). Stated another way, MPC uses a model of the plant to predict future vehicle state evolution and optimise a set of inputs such that this prediction satisfies constraints and minimises a user-defined objective function. At each time step, t, the current plant state is sampled and a cost-minimising control sequence spanning from time t to the end of a control horizon of n sampling intervals, $t + n\Delta t$, is computed subject to inequality constraints. The first element in this input sequence is implemented at the current time and the process is repeated at subsequent time steps.

The vehicle model used in the controller accounts for the kinematics of a 4-wheeled vehicle, along with its lateral and yaw dynamics. Vehicle states include the position of its centre of gravity $[x, y]$, the vehicle yaw angle ψ, yaw rate $\dot{\psi}$, and sideslip angle β, as illustrated in Figure 2. Outputs include lateral position of the c.g. (y) and sideslip at the front wheels (α). Table 1 defines and quantifies this model's parameters.

Figure 2 Vehicle model used in MPC controller

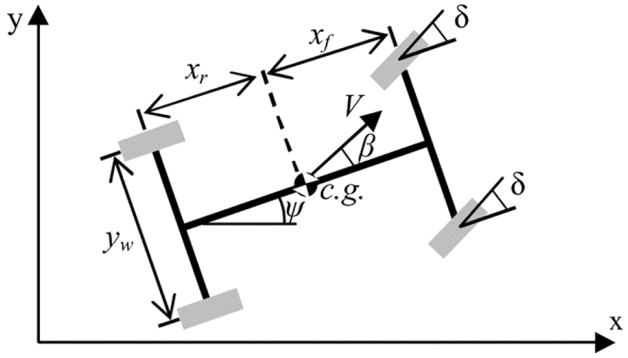

Table 1 Vehicle model parameters

Symbol	*Description*	*Value* [units]
m	Total vehicle mass	2050 [kg]
I_{zz}	Yaw moment of inertia	3344 [kg·m^2]
x_f	C.g. distance to front wheels	1.43 [m]
x_r	C.g. distance to rear wheels	1.47 [m]
y_w	Track width	1.44 [m]
C_f	Front wheel cornering stiffness (linearised about $\alpha_f = 0$)	1433 [N/deg]
C_r	Rear wheel cornering stiffness (linearised about $\alpha_r = 0$)	1433 [N/deg]

Tyre compliance is included in the model by approximating lateral tyre force (F_y) as the product of wheel cornering stiffness ($C(\alpha)$) and wheel sideslip (α or β for front or rear wheels respectively) as shown in equation (15) and illustrated in Figure 3.

$$F_y = C(\alpha)\alpha. \tag{1}$$

Linearised about a constant speed and small slip angles (which will be enforced by the intervention law in hazard avoidance manoeuvres), the equations of motion become

$$\dot{x} = V \tag{2}$$

$$\dot{y} = V(\psi + \beta) \tag{3}$$

$$\dot{\beta} = \frac{-(C_r + C_f)}{mV}\beta + \left(\frac{(C_r x_r - C_f x_f)}{mV^2} - 1\right)\dot{\psi} + \frac{C_f}{mV}\delta \tag{4}$$

$$\ddot{\psi} = \frac{(C_r x_r - C_f x_f)}{I_{zz}}\beta - \frac{(C_r x_r^2 + C_f x_F^2)}{I_{zz}V}\dot{\psi} + \frac{C_f x_f}{I_{zz}}\delta \tag{5}$$

where C_f and C_r represent the (linearised) cornering stiffness of the lumped front wheels and the lumped rear wheels, and x_f and x_r are the longitudinal distances from the c.g. of the front and rear wheels, respectively.

Figure 3 Tyre compliance model illustrating velocity V, slip angle α, lateral force F_y, and cornering stiffness $C(\alpha)$ (see online version for colours)

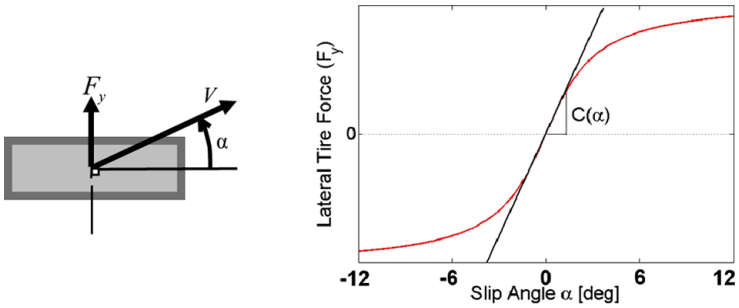

Describing the discretised vehicle plant model by

$$\mathbf{x}_{k+1} = \mathbf{A}\mathbf{x}_k + \mathbf{B}_u\mathbf{u}_k + \mathbf{B}_v\mathbf{v}_k \tag{6}$$

$$\mathbf{y}_k = \mathbf{C}\mathbf{x}_k + \mathbf{D}_v\mathbf{v}_k \tag{7}$$

with $\mathbf{x}$, $\mathbf{y}$, $\mathbf{u}$, and $\mathbf{v}$ representing states, outputs, inputs, and disturbances respectively, a quadratic objective function over a prediction horizon of p sampling intervals is defined as

$$J_k = \sum_{i=k+1}^{k+p}\frac{1}{2}\mathbf{y}_i^{\mathrm{T}}\mathbf{R}_y\mathbf{y}_i + \sum_{i=k}^{k+p-1}\frac{1}{2}\mathbf{u}_i^{\mathrm{T}}\mathbf{R}_u\mathbf{u}_i + \sum_{i=k}^{k+p-1}\frac{1}{2}\Delta\mathbf{u}_i^{\mathrm{T}}\mathbf{R}_{\Delta u}\Delta\mathbf{u}_i + \frac{1}{2}\rho_\varepsilon\varepsilon^2 \tag{8}$$

where $\mathbf{R}_y$, $\mathbf{R}_u$, and $\mathbf{R}_{\Delta u}$ represent diagonal weighting matrices penalising deviations from $\mathbf{y}_i = \mathbf{u}_i = \Delta\mathbf{u}_i = 0$, ρ_ε represents the penalty on constraint violations, n denotes the number

of free control moves, and ε represents the maximum constraint violation over the prediction horizon p. Inequality constraints on vehicle position (**y**), inputs (**u**), and input rates (**Δu**) are defined as:

$$\begin{aligned} \mathbf{y}^j_{\min}(i) - \varepsilon \mathbf{V}^j_{\min}(i) \le \mathbf{y}^j(k+i+1\,|\,k) \le \mathbf{y}^j_{\max}(i) + \varepsilon \mathbf{V}^j_{\max}(i) \\ \mathbf{u}^j_{\min}(i) \le \mathbf{u}^j(k+i+1\,|\,k) \le \mathbf{u}^j_{\max}(i) \\ \Delta\mathbf{u}^j_{\min}(i) \le \Delta\mathbf{u}^j(k+i+1\,|\,k) \le \Delta\mathbf{u}^j_{\max}(i) \\ i = 0, \ldots, p-1 \\ \varepsilon \ge 0 \end{aligned} \tag{9}$$

where the vector Δ**u** represents the change in input from one sampling instant to the next, the superscript '$(\bullet)^j$' represents the jth component of a vector, k represents the current time, and the notation $(\bullet)^j(k + i|k)$ denotes the value predicted for time $k + i$ based on the information available at time k. The vector **V** allows for variable constraint softening over the prediction horizon, p, when ε is included in the objective function.

Assuming that the environment has been delineated previously (see Section 2.1), the boundaries of the traversable road surface ($y_{\min}(x)$ and $y_{\max}(x)$) are sampled over the prediction horizon from t_1 to t_p to generate the constraint vectors

$$\begin{aligned} \mathbf{y}^y_{\max}(k) &= \left[y^y_{\max}(k+1) \quad \ldots \quad y^y_{\max}(k+p) \right]^T \\ \mathbf{y}^y_{\min}(k) &= \left[y^y_{\min}(k+1) \quad \ldots \quad y^y_{\min}(k+p) \right]^T \end{aligned} \tag{10}$$

where $\mathbf{y}^y_{\max}$ and $\mathbf{y}^y_{\min}$ represent the upper and lower limits on the vehicle lateral position (y) as illustrated in Figure 4. These constraints are updated at each sampling interval to account for updates in the host and hazard positions provided by onboard sensing.

Figure 4 Constraint placement ($\mathbf{y}^y_{\max}$, $\mathbf{y}^y_{\min}$) in a straight lane scenario

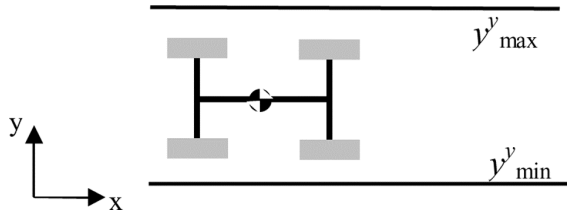

By enforcing vehicle position constraints at the boundaries of the safe region of the road surface,[1] the controller forces the MPC-generated path to remain within the constraint-bounded corridor whenever dynamically feasible. Coupling this lateral position constraint with input constraints, input rate constraints, and vehicle dynamic considerations, the safe operating corridor delineated by $\mathbf{y}^y_{\max}$ and $\mathbf{y}^y_{\min}$ translates to a safe operating 'tube' within the state space (Suh and Bishop, 1987; Langson et al., 2004).

Inside the constraint-bounded tube, various vehicle outputs may be minimised to improve vehicle performance, stability, and controllability. In this work, front wheel sideslip $(\alpha = (x_f / V)\dot{\psi} + \beta - \delta)$ is chosen for its influence on the controllability of front-wheel-steered vehicles. As illustrated in Figure 3, cornering friction begins to decrease above critical slip angles. These critical angles are well-known and provide a direct mapping from environmental conditions to vehicle handling limitations.

The linearised tyre compliance model's failure to account for this decrease further motivates the suppression of front wheel slip angles to reduce controller-plant model mismatch. In Falcone et al. (2007a, 2007b) it is shown that limiting tyre slip angle to avoid this strongly nonlinear (and possibly unstable) region of the tyre force curve can significantly enhance vehicle stability. Further, trajectories that minimise wheel slip also tend to minimise lateral acceleration and yaw rates, leading to a safer and more comfortable ride.

Augmenting the vectors **y**, **u**, Δ**u**, and **v** over the prediction horizon and expressing constraints as

$$\mathbf{A}_c \Delta \mathbf{U}_k \leq \mathbf{b}_c \tag{11}$$

reduces the MPC problem to a quadratic program, which is solved in this work by the two-phase QP solver *LSSOL*. For more details on the MPC problem formulation or solver, the reader is referred to Garcia et al. (1989) and Gill et al. (1986).

2.3 Threat assessment

The vehicle path calculated by the MPC controller is assumed to be the best-case or safest path through the environment. Key metrics from this prediction are therefore used to assess instantaneous threat posed to the vehicle. By setting constraint violation weights (ρ_ε) significantly higher than the competing minimisation weight front wheel sideslip ($\mathbf{R}_\alpha$), a hierarchy of objectives is created to force the constrained optimal solutions to satisfy corridor constraints before minimising front wheel sideslip. When constraints are not active, as illustrated by the grey vehicle in Figure 5, front wheel sideslip – and the corresponding controllability threat – remains at zero. When the solution is constrained, predicted front wheel sideslip increases with the severity of the manoeuvre required to remain within the safe corridor.

Figure 5 Obstacle avoidance scenario showing MPC trajectory plans with varying levels of required front wheel sideslip

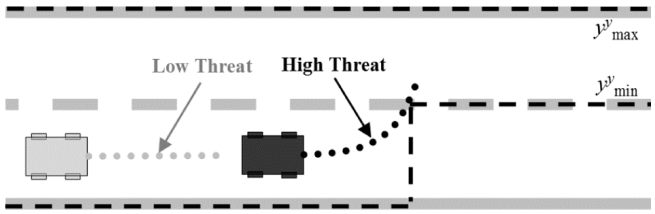

The dark vehicle in Figure 5 illustrates how the MPC-predicted optimal vehicle trajectory might appear as the tyre slip angles and corresponding threat increase in the presence of an active constraint. Physical limits on available tyre cornering friction constrain how large front wheel slip can become before loss of control is imminent (see Figure 3). Thus, the instantaneous vehicle threat may be assessed based on the predicted front wheel sideslip angles required to keep the vehicle within the safe operating corridor.

Various approaches are available to reduce the vector **α** to a scalar threat metric Φ_α. In this work,

$$\Phi_\alpha(k) = \max\left(|\, \alpha_{k+1}, \alpha_{k+2}, \ldots, \alpha_{k+p}\,|\right) \tag{12}$$

was chosen for its good empirical performance when used to regulate controller intervention (described in the next section).

In some scenarios the controller may not completely satisfy roadway position constraints, making α an incomplete indicator of the anticipated threat. These scenarios may arise when abrupt or challenging road corridors cause hard constraints, such as input or input rate, to activate. In these situations, the MPC-predicted vehicle path may violate position constraints, making $\Phi_\alpha = f(\alpha_{\text{predicted}})$ an incomplete threat assessment as it does not capture the additional threat posed by the predicted departure from the safe corridor. To account for such scenarios, an alternative threat metric (similar to the objective function cost) may be used, where

$$\Phi_J(k) = \max \sqrt{\bar{J}_{\text{SI}}(k)} \tag{13}$$

and

$$\bar{J}_{\text{SI}}(k) = \frac{1}{2} R_\alpha \begin{bmatrix} \alpha_{k+1}^2 \\ \alpha_{k+2}^2 \\ \vdots \\ \alpha_{k+p}^2 \end{bmatrix} + \frac{1}{2} R_\delta \begin{bmatrix} \delta_k^2 \\ \delta_{k+1}^2 \\ \vdots \\ \delta_{k+p-1}^2 \end{bmatrix} + \frac{1}{2} R_{\Delta\delta} \begin{bmatrix} \Delta\delta_k^2 \\ \Delta\delta_{k+1}^2 \\ \vdots \\ \Delta\delta_{k+p-1}^2 \end{bmatrix} + \frac{1}{2} \rho_{\text{SI}} \begin{bmatrix} \varepsilon_{k+1}^2 \\ \varepsilon_{k+2}^2 \\ \vdots \\ \varepsilon_{k+p}^2 \end{bmatrix}. \tag{14}$$

This threat metric, while slightly more difficult to interpret physically, accounts for the additive presence of other objective function considerations, such as constraints, input costs, etc, and increases rapidly when constraints are violated. This rate of intervention is tuned independent of the controller cost function by introducing a modified (and adjustable) constraint violation weight, ρ_{SI}.

2.4 Semi-autonomous control

Given a best-case vehicle path through the environment and a corresponding threat, desired inputs from the driver and controller are blended and applied to the vehicle. This blending is performed based on the threat assessment: a low predicted threat causes more of the driver's input and less of the controller's input to be applied to the vehicle, while high threat allows controller input to dominate that of the driver. This "scaled intervention" allows for a smooth transition in control authority from driver to controller as threat increases (and similarly, from controller to driver as threat is reduced).

Denoting the current driver input by u_{dr} and the current controller input by u_{MPC}, the blended input seen by the vehicle, u_v, is defined as

$$u_v = K(\Phi) u_{\text{MPC}} + (1 - K(\Phi)) u_{\text{dr}}. \tag{15}$$

The intervention function $K(\Phi)$ translates predicted vehicle threat Φ into a scalar blending gain $K \in [0\ \ 1]$, defined as

$$K = \begin{cases} 0 & 0 \le \Phi \le \Phi_{\text{eng}} \\ f(\Phi) & \Phi_{\text{eng}} \le \Phi \le \Phi_{\text{aut}} \\ 1 & \Phi \ge \Phi_{\text{aut}} \end{cases}. \tag{16}$$

In equation (16), the shape of K is described by the threat level at which the semi-autonomous controller engages (Φ_{eng}) and the level at which it is given full control

authority and effectively acts as an autonomous controller (Φ_{aut}). When the predicted threat Φ is less than the low-threat threshold Φ_{eng}, K is zero, effectively passing all of the driver's control input (and none of the controller's) to the vehicle. Above the high-threat threshold Φ_{aut}, K is set to one. This allows the MPC controller full control authority to autonomously track the high-threat path. Once the predicted threat is reduced to a safe(r) level (i.e., below Φ_{aut}), the driver's control authority is increased. Figure 6 illustrates linear, piecewise-linear, and nonlinear intervention laws. In this paper, results are presented for piecewise linear formulations parameterised by Φ_{eng} and Φ_{aut} as in equation (17)

$$f(\Phi) = \frac{\Phi_{aut} - \Phi}{\Phi_{aut} - \Phi_{eng}}. \tag{17}$$

When Φ represents the objective function cost, control authority gains become coupled with the 'optimal' MPC solution, thereby ensuring, with an appropriate cost function formulation and choice of ρ_{SI}, that

- the threat metric regulating controller intervention is minimised in the path plan (and associated control calculation)
- the controller maintains complete control authority when constraints are binding.

Figure 6 Intervention laws used to translate threat assessments into controller blending gains

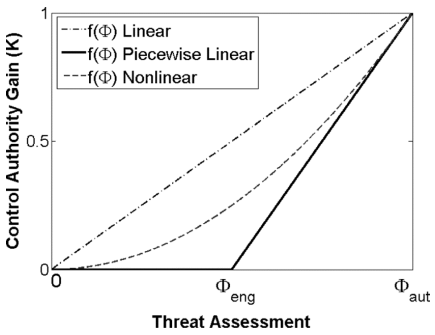

Increasing Φ_{eng} widens the 'low threat' band in which the driver's inputs are unaffected by the controller. While this provides greater driver freedom for low-threat situations, this freedom comes at the cost of increasing the rate of controller intervention when Φ_{eng} is exceeded. This increased rate of intervention may adversely affect driver experience, as discussed in the results below.

Increasing the value of Φ_{aut}, on the other hand, delays complete controller intervention until more severe manoeuvres are predicted. The friction-limited bounds on the linear region of the tyre force curve (1) suggest a natural upper limit of $\Phi_{\alpha} \leq 5$ degrees on surfaces with a friction coefficient of 1.0 in order to ensure that by the time the predicted manoeuvre required to remain within the safe region of the state space reaches this level of severity, the controller has full control authority and can – unless unforeseen constraints dictate otherwise – guide the vehicle to safety.

Using Φ_J to assess threat requires that bounds on $|\alpha|$ be mapped to equivalent $\Phi_{J,eng}$ and $\Phi_{J,aut}$. From equation (8), the mapping of predicted outputs to objective function cost goes as

$$\tilde{\tilde{J}}_{\text{predicted},\vec{y}} = \vec{y}^T \mathbf{R}_y \vec{y} \tag{18}$$

with y representing model outputs, and $\mathbf{R}_y$ representing the output weighting matrix. Table 2 describes the mapping used to render the physical intuition of directly using front-wheel-sideslip for threat assessment to the modified objective function cost approach. Note that due to the additive presence of other objective function considerations such as constraints, input costs, etc., threshold costs $\Phi_{J,\text{eng}}$ and $\Phi_{J,\text{aut}}$ may be reached before the output of interest (α) reaches a critical level.

Table 2 Mapping used to translate threat assessments based on front wheel slip to the equivalent objective-function-cost

	Front wheel sideslip (α)	*Objective function cost* (J)
Prediction variable	$\Phi_\alpha = \text{norm}\lvert\vec{\alpha}\rvert$	$\Phi_J = \sqrt{\text{norm}\lvert\vec{J}_{\text{SI}}\rvert}$
Controller engage threshold $\{K(\Phi_{\text{eng}}) \geq 0\}$	$\Phi_{\alpha,\text{eng}} = \alpha_{\text{eng}}$	$\Phi_{J,\text{eng}} = \sqrt{R_\alpha^2 \alpha_{\text{eng}}^2}$
Autonomous threshold $\{K(\Phi_{\text{aut}}) = 1\}$	$\Phi_{\alpha,\text{aut}} = \alpha_{\text{aut}}$	$\Phi_{J,\text{aut}} = \sqrt{R_\alpha^2 \alpha_{\text{aut}}^2}$

In some scenarios, driver input may differ significantly from controller input. Such cases can lead to abrupt adjustments to steering inputs as K increases. These abrupt changes may saturate steering rate constraints (which are limited by the available steering actuators) and may be uncomfortable and/or unnerving to the human driver. To account for differences between driver and controller input, K may be augmented by an additional term to increase controller intervention in proportion to the driver's deviation from the best-case input. This augmentation can be described by

$$K_{\text{aug}}(\Phi, u_{\text{MPC}}, u_{dr}) = f(\Phi) + (1 - f(\Phi))\left(1 - \text{e}^{\frac{-|u_{\text{MPC}} - u_{dr}|}{\Delta u_{\max}}}\right) \tag{19}$$

where $f(\Phi)$ is defined as in equation (17) and $\Delta u_{\max}$ represents the maximum difference between driver and controller inputs. Figure 7 shows the potential effect of this modification on the intervention law.

Figure 7 Intervention law showing the effect of augmenting K according to driver-controller input deviation

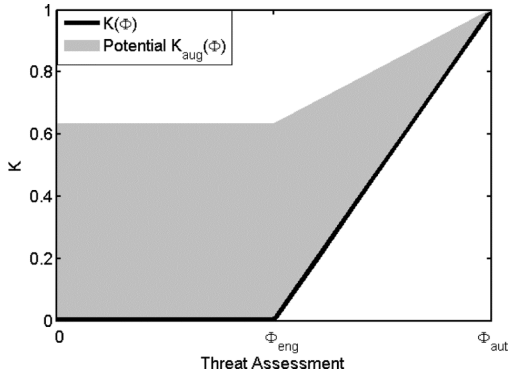

3 Simulation studies

Simulation results were obtained for various manoeuvres, driver inputs, objective function configurations, and intervention laws. Results below are shown for double lane change manoeuvres with a driver steer input $\delta_{driver} = 0$ (intended to simulate a drowsy or inattentive driver) and a constant vehicle velocity of 20 m/s (~72 km/h).

3.1 Setup

A vehicle model similar to the one presented in Keviczky et al. (2006) was used to simulate the plant dynamics. Tyre forces were modelled using a semi-empirical Pacejka tire model, which approximates longitudinal and cornering forces as a function of normal force, tyre slip angle, surface friction, and longitudinal slip. The receding horizon controller used the vehicle model described by equations (2)–(4), with the parameters given in Table 2. Specific controller parameters used in simulated and experimental testing are defined and quantified in Table 3.

Table 3 Controller parameters used in simulation and experiment

Symbol	*Description*	*Value* [*units*]
p	Prediction horizon	35.40
n	Control horizon	18.20
$R_y^{(\alpha)}$	Weight on front wheel slip	0.2657
R_u	Weight on steering input	0.01
$R_{\Delta u}$	Weight on steering input rate (Δ per Δt)	0.01
u_{min}, u_{max}	Min and max constraints on steering input	±10 (degree)
Δu_{min}, Δu_{max}	Min and max constraints on steering input rate (per Δt)	±0.75 (15 degree /s)
y^y_{max} y^y_{min}	Lateral position constraints	Scenario-dependent
ρ_ε	Weight on constraint violation	1×10^5
ρ_{SI}	Modified weight on constraint violation	0.1
$[\Phi_{eng}, \Phi_{aut}]$	Thresholds for controller intervention	[0 3], [1 3], [0 4], [2 4] (degree)
V	Variable constraint softening on lateral vehicle position	[1.25, …, 1.25, 0.01]

3.2 Results

Semi-autonomous intervention using both front wheel sideslip (α) and objective function cost (J) to assess threat were successfully shown to satisfy safety constraints while allowing significant driver control whenever possible. Figure 8 shows the results of semi-autonomous simulations when each metric is used to estimate threat and regulate controller intervention. In each case, $\alpha_{eng} = 0$ and $\alpha_{aut} = 3$ deg, leading to $\Phi_{\alpha, eng} = \Phi_{J, eng} = 0$, $\Phi_{\alpha, aut} = 3$, and $\Phi_{J, aut} = 0.7971$ by the conversion presented in Table 2.

Figure 8 Semi-autonomous double-lane-change simulations showing framework performance when Φ_α and Φ_J are used to assess threat and regulate controller intervention

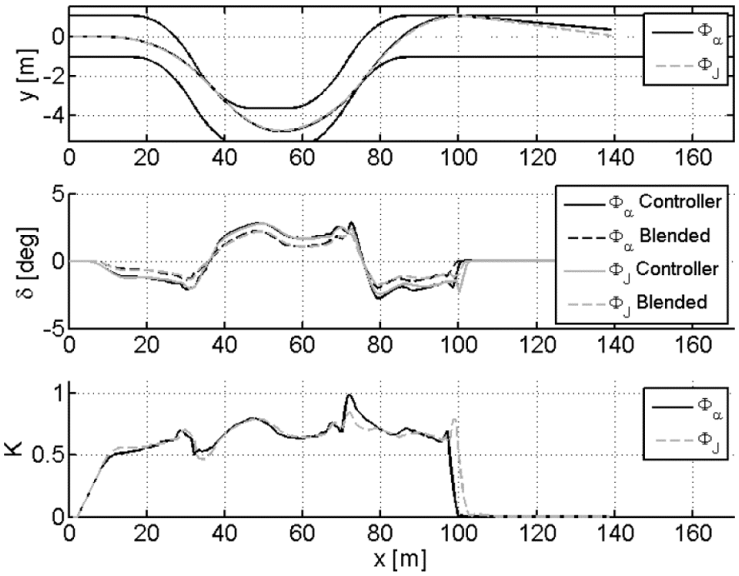

Notice in Figure 8 that threat metrics Φ_α and Φ_J perform similarly when the vehicle trajectory operates far away from constraints. Near constraints, the two diverge, as the additional cost terms in Φ_J ($0.5R_\delta\,\delta^2 + 0.5R_{\Delta\delta}\,\Delta\delta^2 + 0.5\rho_{SI}\,\varepsilon^2$) cause higher peaks in $K = f(\Phi_J)$ than those seen for $K = f(\Phi_\alpha)$.

Intervention laws with varying threat thresholds for controller engagement (α_{eng}) and full autonomy (α_{aut}) were also shown to satisfy lane constraints while honouring driver inputs whenever possible. In the figures below, Φ_α indicates simulations conducted using front wheel slip for the threat assessment while Φ_J indicates simulations that used modified objective function cost. Sideslip thresholds α_{eng} and α_{aut} (in units of degrees) are denoted in figure legends as [α_{eng} α_{aut}] and may be converted to the equivalent threat thresholds Φ_{eng} and Φ_{aut} via the conversion given in Table 2.

As Figures 9 and 10 illustrate, increasing α_{eng} delays controller intervention K at the cost of more rapid increases and more frequent saturation of the control authority allotment. This late intervention, while allowing the human driver greater autonomy far away from constraints/hazards, may ultimately require more control authority to regain control of the vehicle if the driver does not make the necessary correction on their own. For example, increasing α_{eng} from 0 to 2 degrees as shown in Figure 10 ultimately increased the average intervention metric K over the entire manoeuvre by 0.9% for Φ_α-regulated intervention and 7.0% for Φ_J-regulated intervention. Similar results were observed over the entire range of interest in α_{eng} and α_{aut} ($0 \le \alpha_{eng} \le 2$ and $2.5 \le \alpha_{aut} \le 5$), with average intervention K varying by less than 0.09. Figure 11 shows how average K varies with α_{eng} and α_{aut} for this manoeuvre.

Figure 9 Simulation results showing the effect of different intervention thresholds ([α_{eng} α_{aut}] = [0 3], [1 3]) on controller performance using α- and *J*-based threat assessments

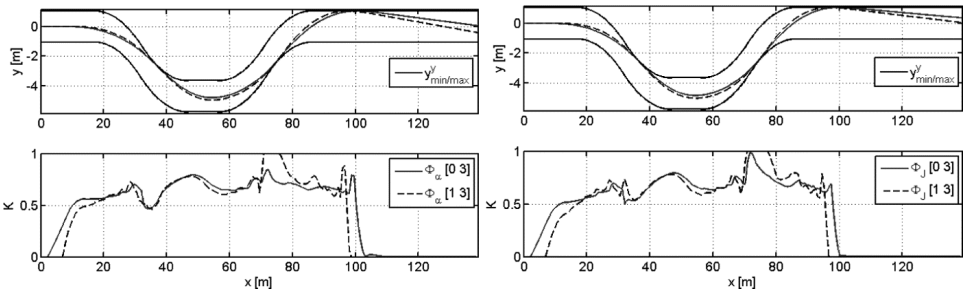

Figure 10 Simulation results showing the effect of different intervention thresholds ([α_{eng} α_{aut}] = [0 4], [2 4]) on vehicle corridor-tracking performance

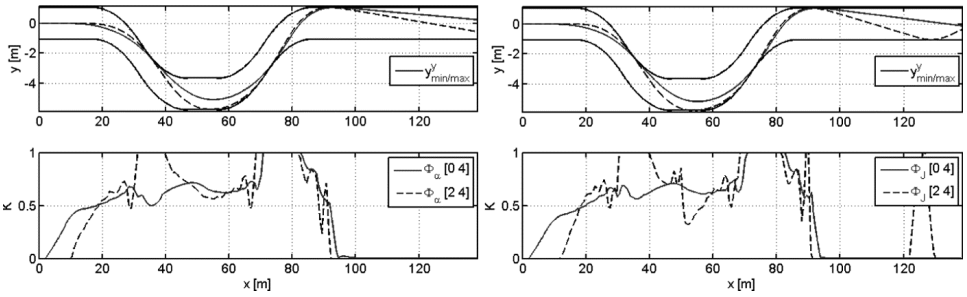

Figure 11 Average intervention *K* for a double lane change with driver steer input input $\delta_{driver} = 0$

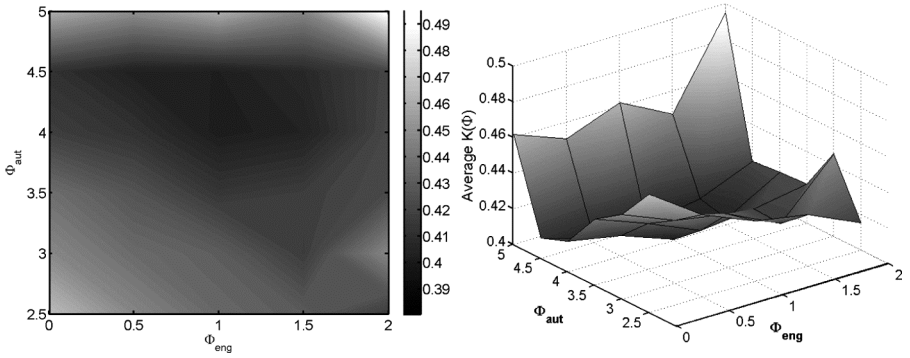

As seen in Figure 11, average controller intervention generally decreases with increasing Φ_{aut} to a point (~4.5 deg). When the controller waits until threat $\Phi_{\alpha} > 4.5$ deg to take full control of the vehicle, the intervention required to keep the vehicle inside the safe corridor increases rapidly due to the rapid decrease in cornering friction near the boundary of the linear tyre force curve (1). This boundary establishes a natural upper limit on Φ_{aut}. Also note that for this scenario, the engagement threshold (Φ_{eng}) could be tuned according to driver preference without significantly affecting average intervention.

Taken together, these results suggest that over the course of some manoeuvres, this framework tends to average out controller intervention for various Φ_{eng} and Φ_{aut} settings, allowing for considerable driver preference tuning without dramatically changing

average K. In this scenario, for example, the maximum change in K across the entire reasonable range of Φ_{eng} and Φ_{aut} was 0.09.

Finally, controller intervention K was shown to satisfy both safety and stability requirements when augmented to account for differences between driver and controller steering inputs via (19). Figure 12 compares a semi-autonomous simulation that does not consider this difference to one that does. Note that large peak values of K combined with small input differences (recall that $\delta_{driver} = 0$) leads to only slight differences in controller intervention for this manoeuvre. In both simulations, $[\alpha_{eng} \ \alpha_{aut}] = [0\ 3]$.

Figure 12 Simulation results showing the effect of augmenting K based on differences between driver and controller steering input

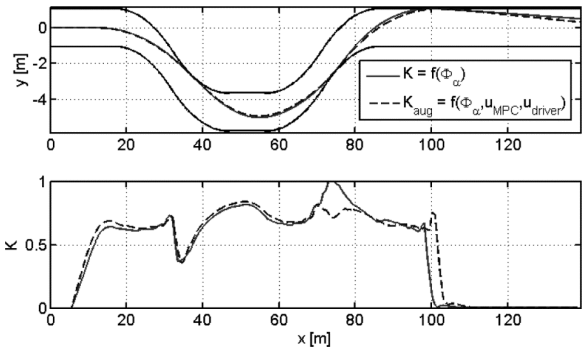

Notice in Figure 12 that for certain manoeuvres, driver inputs, and intervention thresholds Φ_{eng} and Φ_{aut}, augmenting K does not necessarily result in more controller intervention. In the simulation shown above, the opposite is observed owing to the slightly increased intervention early in the manoeuvre, which reduced the subsequent intervention at $x \approx 75$ m.

4 Experimental studies

Experimental testing was performed using a 2001 Jaguar S-Type and three human drivers. Driver and actuator steering inputs were coupled via an Active Front Steer (AFS) system. An inertial and GPS navigation system was used to measure vehicle position, sideslip, yaw angle, and yaw rate while a 1 GHz dSPACE processor ran controller code and interfaced with steering actuators. Prediction and control horizons were chosen as 35–40 and 18–20 timesteps (sampled at 50 ms) respectively to minimise real-time computational overruns of the optimisation routine. Vehicle speed was kept at a relatively-constant 50 km/h to simulate highway driving.

4.1 Manoeuvres

Three common scenarios were used to analyse system performance. In each scenario, obstacles, hazards, and driver targets were represented to the driver by cones and lane markings and to the controller by a constrained corridor (with onboard sensing and constraint mapping assumed to have been performed previously by ‘virtual sensors’ and high-level planners respectively).

Lane keeping experiments tested the threat assessment and intervention characteristics of the controller when the driver manoeuvred inside and outside of the given lane. Six pairs of cones were set up along ~200 metres of the 3.35-metre-wide lane to guide the driver's manoeuvres. As shown in Figure 13 (not to scale), the second- and third sets of cones required the driver to steer the vehicle to the edge of the safe lane while the final two targets required that he attempt to leave the lane. In each of these tests, the driver attempted to remain within the corridor defined by the cones.

Figure 13 Lane keeping test setup showing circles where cones were placed to guide the human driver's (unassisted) path. Lane boundaries delineated by dashed lines were represented as constraints $y^{y}_{\min}$ and $y^{y}_{\max}$ to the controller

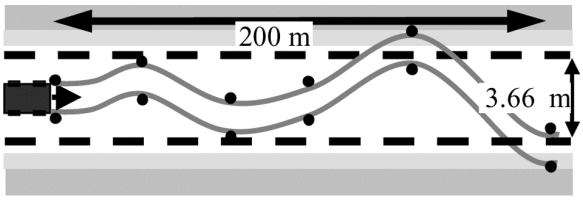

Hazard avoidance tests required that the vehicle avoid an obstacle blocking its original lane of travel. In these tests, the vehicle was driven at a constant velocity in the centre of a lane with the driver holding the steering wheel at $\delta = 0$ as if drowsy or inattentive. A row of cones blocked the vehicle's lane of travel, requiring the controller to:

1 plan a safe lane change manoeuvre around them

2 assess the threat posed by that manoeuvre

3 intervene as necessary to avoid the hazard.

Figure 14 illustrates this test setup.

Figure 14 Hazard avoidance test setup showing hazard cone placement (large circles) and lane boundaries (dashed) enforced by the controller

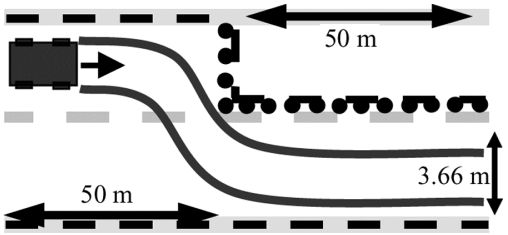

Multiple hazard avoidance experiments tested the controller's ability to navigate more complex road/hazard setups that required manoeuvres with appreciable load transfer. In these tests (illustrated in Figure 15), both lanes of travel were blocked at different locations, forcing the vehicle to change lanes to avoid the first hazard, then change lanes again to avoid the second as in a double-hazard-avoidance manoeuvre.

Figure 15 Multiple hazard avoidance test setup showing hazard cone placement (circles) and lane boundaries (dashed)

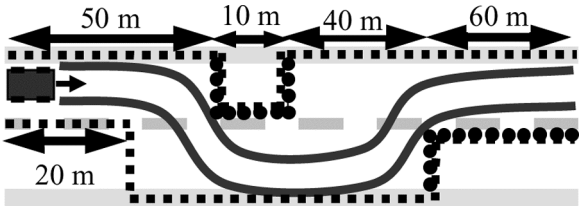

4.2 Controller configuration

Hazard avoidance and multiple hazard avoidance tests were conducted using two different types of driver inputs. Drowsy, inattentive, or otherwise impaired drivers were represented by a constant driver steer input of zero degrees. In these tests, the unassisted driver's path formed a straight line directly through the obstacle(s). To represent active driver steer inputs, the drivers were asked in separate tests to steer either around or into the obstacles. The urgency of these driver steer events was varied – sometimes avoiding the obstacle(s) with a smooth input, others steering at the last minute, and still others, turning the wrong way into an obstacle. Of particular interest in such interactions were the controller's intervention characteristics and its effect on the driver. These effects will be discussed in a follow-on paper.

As explained above, the path plan through a safe environment is determined by adjusting the MPC objective function, constraint setup, and prediction and control horizons. For these experiments, the objective function and constraints were held constant in order to test other framework parameters of interest such as threat assessment and intervention laws. Model and controller parameters used in experiments were the same as those used in simulation (shown in Tables 2 and 3, respectively). Because prediction and control horizons strongly affect path planning, threat assessment, and controller intervention, these were also varied to assess their impact on overall system performance. In general, longer prediction horizons led to smoother optimal vehicle trajectory predictions and, consequently, lower threat assessments. Real time computation limits constrained the feasible prediction (p) and control horizons (n) used in field tests to 40- and 20- sampling periods respectively when 50 ms sampling periods were used. For consistency, only experiments using $p = 40$ and $n = 20$ are shown below. Results obtained using other prediction and control horizons will be discussed in a follow-on paper.

Front wheel sideslip α and modified objective function cost J_{SI} were each tested as threat metrics. Both of these metrics were calculated using the motion plan generated by the MPC algorithm as described by equations (13) and (14).

Various intervention law configurations were tested to determine their effect on vehicle performance and driver experience. These modifications included adjusting threat thresholds Φ_{eng} and Φ_{aut} for controller intervention and augmenting that intervention in proportion to the difference between the driver's current steer input and the controller's desired input (19).

4.3 Results

The semi-autonomous framework proved capable of keeping the vehicle within the safe region of travel for each of the manoeuvres tested and with three different human drivers. The effect of various system parameters on semi-autonomous corridor tracking performance is discussed below.

4.3.1 Manoeuvres

Each of the manoeuvres tested proved feasible for multiple system configurations. Figure 16 shows the results of lane-keeping tests.

Figure 16 Results of semi-autonomously-controlled lane keeping tests

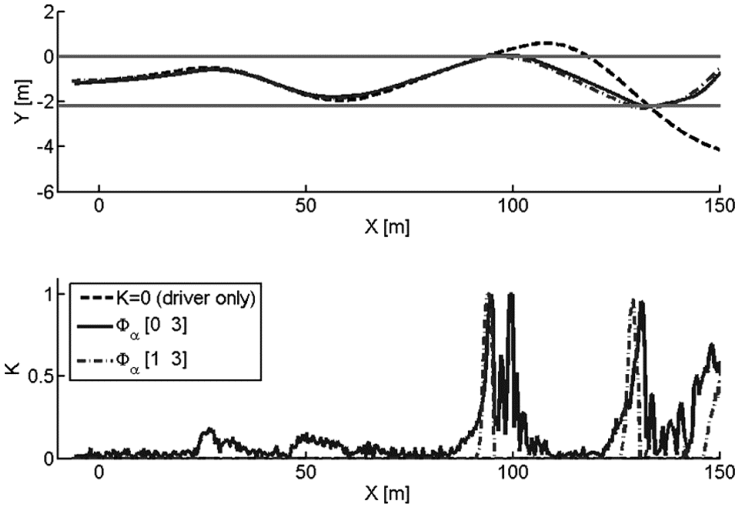

The dashed black line in Figure 16 represents the vehicle trajectory under complete driver control ($K = 0$), and is shown here and in subsequent plots as a reference for the trajectory the driver would have followed had the semi-autonomous controller not engaged. Note that each of the semi-autonomous tests shown above successfully kept the driver within the safe corridor while allowing him significant control authority as long as he remained inside the safe corridor ($x \approx 0$ m to $x \approx 80$ m). Only when the vehicle was about to depart from the corridor did the controller intervene. Each of these interventions was early and large enough to arrest departure from the safe corridor. The slight intervention observed between $x \approx 20$ m and $x \approx 60$ m illustrates the framework's response to a predicted trajectory that required appreciable sideslip in order to remain within the lane. When the driver corrected the vehicle heading, K returned to approximately zero. Note further that increasing Φ_{eng} from 0 to 1 degrees effectively eliminates low-threat intervention noise.

Figure 17 shows the results of multiple hazard avoidance experiments.

Figure 17 Results of driver-controlled, autonomously-controlled, and semi-autonomously-controlled hazard avoidance tests

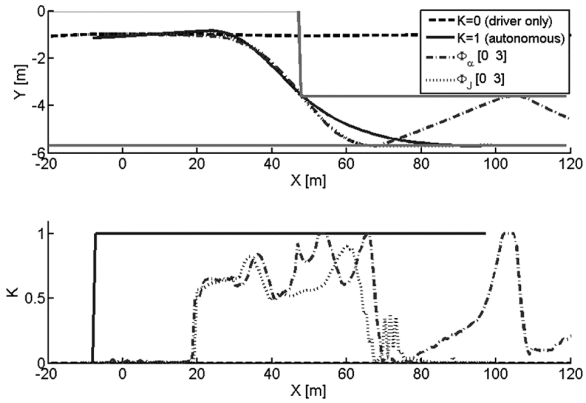

Notice that in each experiment, the controller did not interfere with the driver's natural/unassisted trajectory in low-threat situations. When it did intervene, it allocated enough control authority to the controller to avert safe lane departure or loss of control. Note that the trajectory oscillation observed in the Φ_α-regulated experiment was a result of an overcorrection on the part of the controller at $x \sim 65$ m. The vehicle trajectory proceeded to rebound from of $y^y_{\max}$ because the driver's input remained at $\delta_{\text{driver}} = 0$. Were the driver more attentive as a result of the first intervention incident, the low levels of K directly following the initial rebound would have allowed him significant control authority to correct and straighten out the vehicle.

Figure 17 also shows the results of an autonomous experiment in which the controller was given full control authority ($K = 1$). Notice that for the given driver input ($\delta_{\text{driver}} = 0$), the vehicle path under semi-autonomous control closely resembles the 'best case' path achieved using autonomous control while exerting only an average intervention level (K) of 0.40 and 0.28 for Φ_α- and Φ_J- regulated intervention, respectively.

Figure 18 shows the results of multiple hazard avoidance experiments controlled by a human driver only (dashed), the autonomous framework only ($K = 1$, solid), and the semi-autonomous combination of driver and controller (dashed-dot and dotted).

Figure 18 Results of multiple hazard avoidance tests showing the effect of K augmentation on the vehicle trajectory

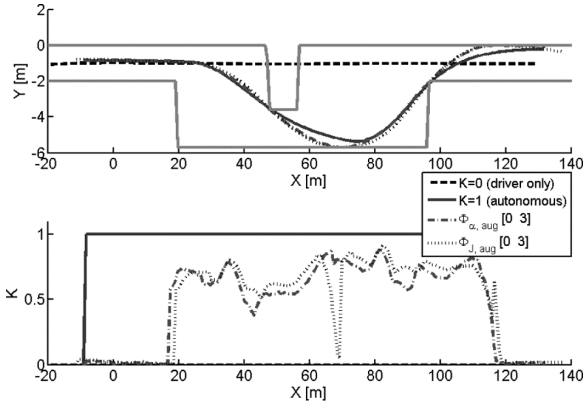

As observed with lane-keeping and hazard avoidance tests, each of these experiments successfully kept the vehicle within the safe road corridor. Notice again that even with the input blending required for semi-autonomous implementation, each semi-autonomous trajectory closely resembled the objective-function-optimal path taken by the autonomous controller.

4.3.2 Intervention laws

Good experimental results were obtained using both front wheel slip Φ_α and objective function cost Φ_J as threat metrics. Figure 19 compares two such experiments to tests using zero intervention (dashed) and autonomous control (solid).

Figure 19 Results of multiple hazard avoidance tests using Φ_α- and Φ_J-based threat assessments to govern controller intervention

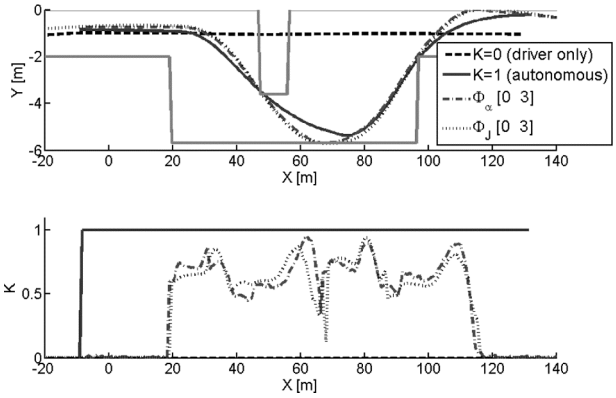

Various threat thresholds for engaging (Φ_{eng}) and saturating (Φ_{aut}) the control authority of the autonomous controller (K) were also successfully tested and shown to avoid hazards under a range of driver inputs. Figure 20 compares a semi-autonomous multi-hazard-avoidance manoeuvre without an intervention 'deadband' ($\Phi_{eng} = 0$) to an otherwise identical scenario using a deadband ($\Phi_{eng} = 1°$).

Figure 20 Multiple hazard avoidance manoeuvre showing the effect of increasing Φ_{eng} to allow for a controller 'deadband' in low-threat predicted manoeuvres

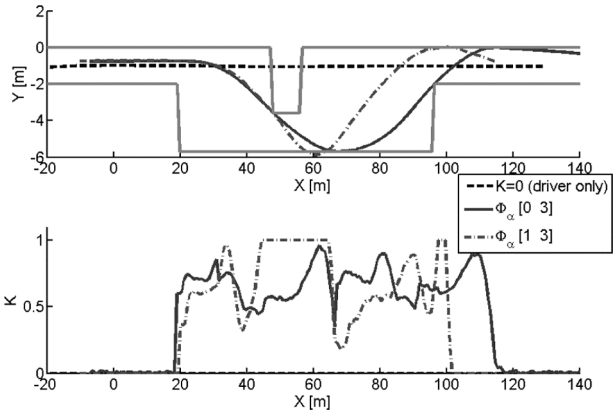

While this deadband delays initial controller intervention, it also leads to more severe (faster and larger) spikes in K, which were generally found to be uncomfortable to the human driver. This result was consistent with simulated tests. That is, larger deadbands in K lead to necessarily greater rate of change in $K(\Phi)$, which in turn leads to less controller intervention during low threat manoeuvres and rapid increases in intervention once the predicted threat surpasses the engagement threshold. Note that for the experiment with a deadband (dash-dot), the delay in controller intervention led to a slight violation of the safe lane of travel and a corresponding saturation of the control authority allocated to the controller. These rapid intervention events were generally unnerving to the human driver.

Intervention laws considering driver input via (19) were also shown to effectively allocate control authority. Figure 21 shows how augmenting intervention gains based on both Φ_α and Φ_J affected semi-autonomous controller performance.

Figure 21 Results of multiple hazard avoidance tests showing the effect of K augmentation on the vehicle trajectory when intervention is based on Φ_α and Φ_J

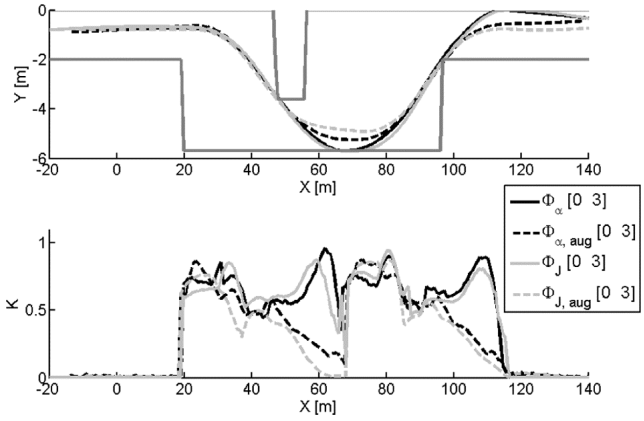

Note from Figure 21 that in this particular scenario, the effect of K augmentation on controller intervention and vehicle performance appears more pronounced than the effect of using different threat assessments (Φ_α vs. Φ_J). This is consistent with the observation that for less demanding manoeuvres (i.e., those which can be accomplished without violating lane constraints), the objective function cost is almost exclusively a function of front wheel slip and performs similarly to the front-slip-modulated configuration. When these configurations are augmented via (19), initial intervention, K, increases, allowing a subsequently smoother trajectory which ultimately requires less controller intervention (average K) altogether. Test drivers generally preferred the smooth control authority transition provided by this augmented intervention function.

Finally, Figures 17–21 above show multiple hazard avoidance scenarios in which the driver input remained at zero. Experiments were also conducted in which the driver was instructed to swerve at the last minute to avoid hazards. Two such scenarios are shown in Figure 22.

Notice that in both semi-autonomous cases, controller intervention slightly preceded an otherwise-late driver reaction. The combined effect of both inputs was then sufficient to avoid both road hazards.

Figure 22 Results of multiple hazard avoidance tests in which the driver swerved to avoid hazards

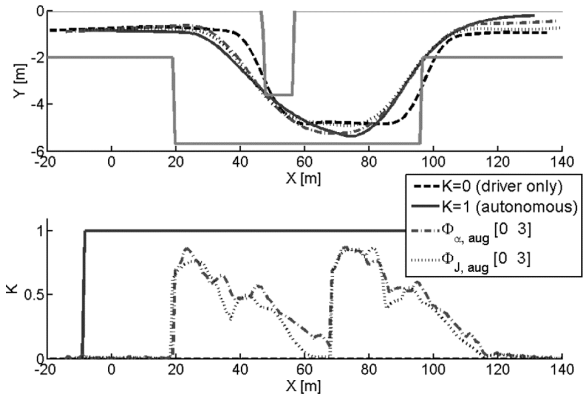

In each of the above experimental results, this shared-adaptive controller behaves as a stable closed-loop system. While this was also true of all of the other simulated and experimental results conducted to date, no rigorous stability proof is presented in this paper; this is a topic of current investigation.

5 Conclusions

This paper presented an optimal-control-based framework that performs trajectory planning, threat assessment, and semi-autonomous control of passenger vehicles in hazard avoidance scenarios. This framework has been tested in simulations and experiments and has proven capable of avoiding hazards while sharing control with a human driver using multiple threat metrics and intervention laws. Additionally, this framework has been shown to provide significant autonomy to a human driver, intervening only as necessary to keep the vehicle under control and within the safe roadway corridor. Simulated and experimental results have also shown this control framework to be stable even in the presence of system-inherent time delays, though a rigorous stability proof is a topic of current investigation.

Finally, while human factors have not been studied in depth here, it is expected that with additional investigation, a best-case, or average driver-preferred intervention law may be described and intervention settings tuned accordingly. Further work is needed before this research is road-ready.

References

Ackermann, J. (1994) 'Robust decoupling of car steering dynamics with arbitrary mass distribution', *Proceedings of the 1994 American Control Conference. Part 2 (of 3)*, Green Valley, AZ, American Automatic Control Council, 29 June–1 July, USA, pp.1964–1968.

Alleyne, A. (1997a) 'A comparison of alternative obstacle avoidance strategies for vehicle control', *Vehicle System Dynamics*, Vol. 27, Nos. 5–6, pp.371–392.

Alleyne, A. (1997b) 'Comparison of alternative intervention strategies for unintended roadway departure (URD) control', *Vehicle System Dynamics*, Vol. 27, No. 3, pp.157–186.

Bemporad, A., Morari, M., Dua, V. and Pistikopoulos, E. (2002) 'The explicit linear quadratic regulator for constrained systems', *Automatica*, Vol. 38, No. 1, pp.3–20.

Besselmann, T. and Morari, M. (2008) 'Hybrid parameter-varying model predictive control for autonomous vehicle steering', *European Journal of Control*, Vol. 14, No. 5, pp.418–431.

Borrelli, F., Falcone, P., Keviczky, T., Asgari, J. and Hrovat D. (2005) 'MPC-based approach to active steering for autonomous vehicle systems', *International Journal of Vehicle Autonomous Systems*, Vol. 3, Nos. 2–4, pp.265–291.

Brandt, T., Sattel, T. and Bohm, M. (2007) 'Combining haptic human-machine interaction with predictive path planning for lane-keeping and collision avoidance systems', *2007 IEEE Intelligent Vehicles Symposium, IV 2007*, Institute of Electrical and Electronics Engineers Inc., 13–15 June, Piscataway, NJ 08855-1331, USA, pp.582–587.

Calhoun, P.C. and Queen, E.M. (2002) 'Entry vehicle control system design for the mars smart Lander', *Presented at the AIAA Atmospheric Flight Mech. Conf.*, Monterey, CA.

Camacho, E.F. and Bordons, C. (2004) *Model Predictive Control*, 2nd ed., Springer, New York, NY, USA.

Cremean, L.B., Foote, T.B., Gillula, J.H., Hines, G.H., Kogan, D., Kriechbaum, K., Lamb, J., Leibs, J., Lindzey, L., Rasmussen, C., Stewart, A., Burdick, J.W. and Murray, R.M. (2006) 'Alice: An information-rich autonomous vehicle for high-speed desert navigation', *Journal Field Robotics*, Vol. 23, No. 9, pp.777–810.

Engelman, G., Ekmark, J., Tellis, L., Tarabishy, M.N., Joh, G.M., Trombley, R.A. and Williams, R.E. (2006) *Threat Level Identification and Quantifying System*, US Patent 7034668 B2.

Falcone, P., Borrelli, F., Tseng, H., Asgari, J. and Hrovat, D. (2008a) 'A hierarchical model predictive control framework for autonomous ground vehicles', *Proceedings of the 2008 American Control Conference, ACC*, Piscataway, Institute of Electrical and Electronics Engineers Inc., 11–13 June, NJ 08855-1331, USA, pp.3719–3724.

Falcone, P., Borrelli, F., Tseng, H., Asgari, J. and Hrovat, D. (2008b) 'A linear time varying model predictive control approach to the integrated vehicle dynamics control problem in autonomous systems', *Proceedings of the 46th IEEE Conference on Decision and Control 2007, CDC*, Institute of Electrical and Electronics Engineers Inc., 12–14 December, 2007, Piscataway, NJ 08855-1331, USA, pp.2980–2985.

Falcone, P., Borrelli, F., Tseng, H.E., Asgari, J. and Hrovat, D. (2007a) 'Predictive active steering control for autonomous vehicle systems', *IEEE Transactions on Control Systems Technology*, Vol. 15, No. 3, pp.566–580.

Falcone, P., Borrelli, F., Tseng, H.E., Asgari, J. and Hrovat, D. (2007b) 'Integrated braking and steering model predictive control approach in autonomous vehicles', *5th IFAC Symposium on Advances in Automotive Control*, Berkeley, CA.

Falcone, P., Tseng, H.E., Borrelli, F., Asgari, J. and Hrovat, D. (2008c) 'MPC-based yaw and lateral stabilisation via active front steering and braking', *Vehicle System Dynamics*, Vol. 46, Suppl1, pp.611–628.

Fritsch, J., Michalke, T., Gepperth, A., Bone, S., Waibel, F., Kleinehagenbrock, M., Gayko, J. and Goerick, C. (2008) 'Towards a human-like vision system for driver assistance', *Intelligent Vehicles Symposium, 2008 IEEE*, Eindhoven, Netherlands, pp.275–282.

Fritz, H., Gern, A., Schiemenz, H. and Bonnet, C. (2004) 'CHAUFFEUR assistant – a driver assistance system for commercial vehicles based on fusion of advanced ACC and lane keeping', *Proceedings of the 2004 IEEE Intelligent Vehicles Symposium*, Institute of Electrical and Electronics Engineers Inc., 14–17 June, Piscataway, NJ 08855-1331, USA, pp.495–500.

Garcia, C., Prett, D. and Morari, M. (1989) 'Model predictive control: theory and practice – a survey', *Automatica*, Vol. 25, No. 3, pp.335–348.

Gill, P.E., Hammarling, S.J., Murray, W., Saunders, M.A. and Wright, M. (1986) *User's Guide for LSSOL (Version 1.0): A FORTRAN Package for Constrained Linear Least-cquares and Convex Quadratic Programming*, Dept. of Operations Research: Stanford University, Stanford, California 94305.

Guo, L., Wang, J. and Li, K. (2006) 'Lane keeping system based on THASV-II platform', *IEEE International Conference on Vehicular Electronics and Safety, ICVES 2006*, Institute of Electrical and Electronics Engineers Computer Society, December, Piscataway, NJ 08855-1331, USA, pp.305–308.

Jansson, J. (2005) *Collision Avoidance Theory with Application to Automotive Collision Mitigation*, Doctoral Dissertation, Linkoping University, SE-581 83 Linköping, Sweden.

Keviczky, T., Falcone, P., Borrelli, F., Asgari, J. and Hrovat, D. (2006) 'Predictive control approach to autonomous vehicle steering', *Proceedings of the 2006 American Control Conference*, Institute of Electrical and Electronics Engineers Inc., 14–16 June, Piscataway, NJ 08855-1331, USA, pp.4670–4675.

Langson, W., Chryssochoos, I., Rakovic, W. and Mayne, D. (2004) 'Robust model predictive control using tubes', *Automatica*, Vol. 40, No.1, pp.125–133.

Lemelson, J.H. and Pedersen, R.D. (1999) *GPS Vehicle Collision Avoidance Warning and Control System and Method*, US Patent 5983161.

Leonard, J., How, J., Teller, S., Berger, M., Campbell, S., Fiore, G., Fletcher, L., Frazzoli, E., Huang, A., Karman, S., Koch, O., Kuwata, Y., Moore, D., Olson, E., Peters, S., Teo, J., Truax, R., Walter, M., Barrett, D., Epstein, A., Maheloni, K., Moyer, K., Jones, T., Buckley, R., Antone, M., Galejs, R., Krishnamurthy, S. and Willilams, J. (2008) 'A perception-driven autonomous urban vehicle', *Journal Field Robotics*, Vol. 25, No. 10, pp.727–774.

Liu, J., Wu, J. and Su, Y. (2007) 'Development of an interactive lane keeping control system for vehicle', *VPPC 2007 – Proceedings of the 2007 IEEE Vehicle Power and Propulsion Conference*, Institute of Electrical and Electronics Engineers Computer Society, 9–12 September, Piscataway, NJ 08855-1331, USA, pp.702–706.

McBride, J.R., Ivan, J.C., Rhode, D.S., Rupp, J.D., Rupp, M.Y., Higgins, J.D., Turner, D.D. and Eustice R.M. (2008) 'A perspective on emerging automotive safety applications, derived from lessons learned through participation in the DARPA grand challenges', *Journal Field Robotics*, Vol. 25, No. 10, pp.808–840.

Mobus, R. and Zomotor, Z. (2005) 'Constrained optimal control for lateral vehicle guidance', *2005 IEEE Intelligent Vehicles Symposium Proceedings (IEEE Cat. No. 05TH8792)*, 6–8 June, Piscataway, NJ, IEEE, USA, pp.429–434.

National Highway Traffic Safety Administration (NHTSA) (2008) *2007 Traffic Safety Annual Assessment – Highlights*, NHTSA National Center for Statistics and Analysis, Washington DC 20590.

Netto, M., Blosseville, J., Lusetti, B. and Mammar, S. (2006) 'A new robust control system with optimized use of the lane detection data for vehicle full lateral control under strong curvatures', *ITSC 2006: 2006 IEEE Intelligent Transportation Systems Conference*, Institute of Electrical and Electronics Engineers Inc., 17–20 September, Piscataway, NJ 08855-1331, USA, pp.1382–1387.

Pilutti, T. and Ulsoy, A.G. (1999) 'Identification of driver state for lane-keeping tasks', *IEEE Transactions on Systems, Man, and Cybernetics Part A: Systems and Humans.*, Vol. 29, No. 5, pp.786–502.

Pilutti, T., Ulsoy, G. and Hrovat, D. (1995) 'Vehicle steering intervention through differential braking', *Proceedings of the 1995 American Control Conference*, Seattle, WA, USA, 21–23 June, pp.1667–1671.

Pohl, J., Birk, W. and Westervall, L. (2007) 'A driver-distraction-based lane-keeping assistance system', *Proceedings of the Institution of Mechanical Engineers. Part I: Journal of Systems and Control Engineering*, Vol. 221, No. 4, pp.541–552.

Rossetter, E.J. and Christian Gardes, J. (2006) 'Lyapunov based performance guarantees for the potential field lane-keeping assistance system' *Journal of Dynamic Systems, Measurement and Control, Transactions of the ASME*, Vol. 128, No. 3, pp.510–522.

Sattel, T. and Brandt, T. (2008) 'From robotics to automotive: Lane-keeping and collision avoidance based on elastic bands', *Vehicle System Dynamics*, Vol. 46, No. 7, pp.597–619.

Smith, R.S., Mease, K.D., Bayard, D.S. and Farless, D.L. (2000) 'Aeromaneuvering in the martian atmosphere: simulation-based analyses', *Journal of Spacecraft and Rockets*, Vol. 37, No. 1, pp.139–142.

Suh, S. and Bishop, A.B. (1987) 'Tube concept and its application to the obstacle-avoiding minimum-time trajectory planning problem', *Proceedings of the 1987 IEEE International Conference on Systems, Man and Cybernetics*, IEEE, New York, NY, USA, pp.14–20.

Tan, C., Sutton, R. and Chudley, J. (2007) 'An integrated collision avoidance system for autonomous underwater vehicles', *International Journal of Control*, Vol. 80, No. 7, pp.1027–1049.

Thrun, S., Montemerlo, M., Dahlkamp, H., Stavens, D., Aron, A., Diebel, J., Fong, P., Gale, J., Halpenny, M., Hoffmann, G., Lau, K., Oakley, C., Palatucci, M., Pratt, V., Stang, P., Strohband, S., Dupont, C., Jendrossek, L., Koelen, C., Markey, C., Rummel, C., van Niekerk, J., Jensen, E., Alessandrini, P., Bradski, G., Davies, B., Ettinger, S., Kaehler, Ad., Nefian, A. and Mahoney, P. (2006) 'Stanley: The robot that won the DARPA grand challenge', *Journal of Field Robotics*, Vol. 23, No. 9, pp.661–692.

Tsourveloudis, N., Valavanis, K. and Hebert, T. (2001) 'Autonomous vehicle navigation utilizing electrostatic potential fields and fuzzy logic', *IEEE Transactions on Robotics and Automation*, Vol. 17, No. 4, pp.490–497.

Vaidyanathan, R., Hocaoglu, C., Prince, T.S. and Quinn, R.D. (2001) 'Evolutionary path planning for autonomous air vehicles using multiresolution path representation', *2001 IEEE/RSJ International Conference on Intelligent Robots and Systems*, Institute of Electrical and Electronics Engineers Inc., Maui, HI, USA, 29 October– 3 November, pp.69–76.

Weilkes, M., Burkle, L., Rentschler, T. and Scherl, M. (2005) 'Future vehicle guidance assistance – combined longitudinal and lateral control', *Automatisierungstechnik*, Vol. 42, No. 1, pp.4–10.

Wei-Min, L. and Bayard, D.S. (1999) 'Guidance and control for Mars atmospheric entry: adaptivity and robustness', *Proceedings of the 14th World Congress of IFAC 99*, International Federation of Automatic Control, Kidlington, Elsevier Sci, 5–9 July, UK, pp.383–388.

Yu, H., Spenko, M. and Dubowsky, S. (2003) 'An adaptive shared control system for an intelligent mobility aid for the elderly', *Autonomous Robots*, Vol. 15, No. 1, pp.53–66.

Zheng, N., Tang, S., Cheng, H., Li, Q., Lai, G. and Wang, F. (2004) 'Toward intelligent driver-assistance and safety warning system', *IEEE Intelligent Systems*, Vol. 19, No. 2, pp.8–11.

Zomotor, Z. and Franke, U. (1997) 'Sensor fusion for improved vision based lane recognition and object tracking with range-finders', *Proceedings of the 1997 IEEE Conference on Intelligent Transportation Systems, ITSC*, Piscataway, IEEE, 9–12 November, NJ, USA, pp.595–600.

Note

[1]Position constraints may be applied to vehicle profile or offset and applied to the centre of gravity. See The Appendix for an explanation of each approach.

Appendix

Position constraints may be placed on the vehicle's physical profile or on its centre of gravity. In the first approach, nodes are defined on the vehicle perimeter and forced to remain within the constraints y_{min} and y_{max}. Figure A1 illustrates this constraint placement using nodes A, B, C, and D and defining four constrained outputs y_A, y_B, y_C, and y_D. Equation A1 shows the linearised (about $\psi = 0$) form of the corresponding output equations.

$$\begin{bmatrix} y_A \\ y_B \\ y_C \\ y_D \end{bmatrix} = \begin{bmatrix} 0 & 0 & d_f & 1 \\ 0 & 0 & d_f & 1 \\ 0 & 0 & -d_r & 1 \\ 0 & 0 & -d_r & 1 \end{bmatrix} \begin{bmatrix} \beta \\ \dot{\psi} \\ \psi \\ y \end{bmatrix} + \begin{bmatrix} 1 \\ -1 \\ -1 \\ 1 \end{bmatrix} w \tag{A1}$$

Figure A1 Constraint enforcement using perimeter nodes (see online version for colours)

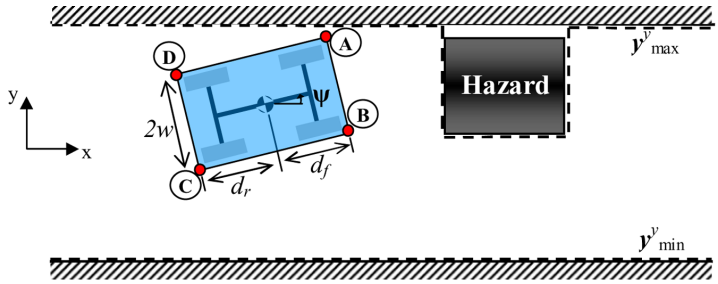

In the simulations and experiments presented in this paper, the vehicle centre of gravity was constrained to remain within a restricted corridor. Note from equation A1 that for small yaw angles (all of the experiments shown above exhibited $\psi < 6°$), the vehicle perimeter may be roughly accounted for by shifting vertical and horizontal constraints by $w + \varepsilon$ and $d_f + \delta$, respectively, where ε and δ were chosen to provide a small buffer against non-zero yaw. In this work, $\varepsilon = \delta \approx 0.2$ m. For experiments in which human drivers actively sought to avoid hazards, hazard cones were offset from corridor constraints so as to provide a visual representation of the corresponding hazard to the human driver. Figure A2 illustrates these offsets. Controller performance in these experiments was also evaluated based on its ability (as clearly observed in data logs) to keep the centre of gravity from violating the (offset) position constraints.

Figure A2 Constraint placement using corridor offsets (see online version for colours)